Geophysical Prospecting

EAGE EUROPEAN ASSOCIATION OF GEOSCIENTISTS & ENGINEERS

Geophysical Prospecting, 2010, 58, 321–334 doi: 10.1111/j.1365-2478.2009.00817.x

Magnetic basement: gravity-guided magnetic source depth analysis and interpretation

Serguei A. Goussev[1*] and John W. Peirce[2]

[1]*Fugro Robertson Inc., Gravity & Magnetic Services, 6100 Hillcroft, 5th Floor, PO Box 740010, Houston, TX 77274, USA, and* [2]*GEDCO, 815 8th Avenue SW, Suite 1200, Calgary T2P 3P2, Alberta, Canada*

Received December 2007, revision accepted May 2009

ABSTRACT

We present a new integrated approach to the interpretation of magnetic basement that is based on recognition of characteristic patterns in distributions and alignments of magnetic source depth solutions above and below the surface of magnetic basement. This approach integrates a quantitative analysis of depth solutions, obtained by 2D Werner deconvolution of the magnetic data, with a qualitative evaluation of the Bouguer gravity anomalies. The crystalline/metamorphic basement and sedimentary cover have different origins, tectonic histories, lithologies and magnetic properties. These differences result in different geometries of magnetic sources associated with faults, fracture zones, igneous intrusions, erosional truncations, subcrop edges and other structural discontinuities.

Properly tuned, 2D Werner deconvolution is able to resolve the intra-sedimentary and intra-basement magnetic source geometries into distinctly different distributions and alignments of calculated depth solutions. An empirical set of criteria, basement indicators, was developed for identification and correlation of the basement surface. The ambiguity of basement correlation with limited or non-existent well control, which is common for onshore frontier and offshore explorations, can be reduced by incorporating the Bouguer gravity data into the process of correlation.

INTRODUCTION

There are two main approaches to the mapping of the magnetic basement: depth-to-magnetic source analysis and 3D modelling with subsequent structural inversion.

Magnetic basement mapping with the depth-to-magnetic source techniques has been in use for several decades. The working concept is that dominant anomalies in the observed magnetic field are generated by sources near the basement top (Nabighian *et al.* 2005). There are several proven techniques, both manual and automated, which provide calculations of the magnetic source depth solutions (Li 2003). Different methods work best for different simplified source geometries like thin dike, contact, sphere, horizontal or vertical cylinder, etc. Manual/graphical methods relate the magnetic source depth to the measured distances between characteristic points of the anomaly's profile. The automated methods, like 2D Werner deconvolution (Werner 1955), work on profiles of the magnetic data. Those algorithms, using simplified source geometry approximations and different calculation parameters (clustering, regional interference, length of calculating window), solve a system of redundant equations for magnetic source parameters, including location and depth. The complicating factors for determination of basement depth are noise contamination, interference of adjacent anomalies and igneous material in the sedimentary section. The calculated depths to the tops of intra-sedimentary magmatic intrusions and volcanics will differ significantly from the actual basement depth but may often be misinterpreted as basement. Often, the sparse distribution of 'reliable' depth solutions means that the accuracy and lateral resolution of the basement interpretation is much less than the expectations of petroleum exploration in structurally complex areas.

*E-mail: sgoussev@fugro.com

3D modelling and structural inversion are based on construction of a 3D magnetic and/or gravity model of the subsurface from available data that can be inverted for the basement depth (Nabighian *et al.* 2005). The working concept is that the model misfit (i.e., difference between the observed magnetic or gravity field and the field calculated from the constructed 3D model) can be assigned to unknown variations of the basement depth and, hence, inverted for it. The accuracy and lateral resolution of 3D structural inversion are strongly dependent on information about magnetic susceptibility and density of basement rocks and the initial basement structure chosen. Such information is usually very limited or not available and that makes a poorly constrained 3D structural inversion subject to large possible errors.

In the mid-90s, one of us (JWP) proposed a new approach to magnetic basement interpretation from the high-resolution aeromagnetic (HRAM) data that was used extensively in the Western Canada Sedimentary Basin. This approach is based on experience of a visual analysis and recognition of characteristic patterns in distributions and alignments of magnetic depth solutions, obtained by 2D Werner automated depth-to-source estimation technique, near wells that penetrated the crystalline/metamorphic basement. The analysis revealed consistent and repeated changes in distributions and alignments of calculated magnetic source depth solutions across the surface of magnetic basement. In many areas we had good control from basement wells to constrain the interpretation and to calibrate our early interpretations. In the search for an explanation of these empirical observations, we have found three types of corroborating evidence, described below as the 'geologic', 'magnetic' and 'synthetic modelling' evidences. Based on experience of application under various structural-geological environments, an empirical set of basement indicators was developed for identification and correlation of the basement surface using available well control. However, in frontier areas, both onshore and offshore, wells that reach basement are few or non-existent. This lack of well control can be, in part, compensated by integration with the Bouguer gravity data. Usually, the gravity data are acquired in marine acquisition concurrently with the magnetic data. Onshore gravity data may be available from ground or airborne surveys.

METHODOLOGY

There are three definitions of the basement used in petroleum exploration: geologic, magnetic and acoustic. Often, these terms are used loosely and interchangeably although they have distinctly different meanings.

By definition of the Glossary of Geology (Neuendorf, Mehl and Jackson 2005, p. 57), the geologic basement is "the crust of the Earth below sedimentary deposits, extending downward to the Mohorovicic discontinuity. In many places the rocks are igneous and metamorphic and of Precambrian age, but in some places they are Paleozoic, Mesozoic or even Cenozoic". The magnetic basement is "the upper surface of extensive heterogeneous rocks having relatively large magnetic susceptibilities compared with those of sediments; often but not necessarily coincident with the geologic basement" (ibid, p. 389).

By definition of the Encyclopedic Dictionary of Applied Geophysics (Sheriff 2006, p. 2), the acoustic basement is "the deepest more-or-less continuous seismic reflector; often an unconformity below which seismic energy returns are poor or absent. Also called seismic basement".

For the purposes of our approach, it should be noted that a) geologic basement and magnetic basement can be but are not necessarily, the same geological boundary and b) acoustic basement, which is often used as an upper constraint for the magnetic basement interpretation, can be structurally close or coincident with the magnetic basement, or it can be much shallower than magnetic basement (for example, top of tight carbonates). If there is little velocity contrast between the lowermost sediments and basement, then the basement itself is unlikely to show as a clear acoustic basement reflector.

From several automated depth-to-source estimation techniques, proven to be reliable and efficient in application for the last 20–25 years, we use 2D Werner deconvolution developed by Werner (1955) and automated by Hartman, Teskey and Friedberg (1971) and Ku and Sharp (1983) for the line-by-line magnetic source depth calculations. We run multiple window calculations for both the total field (thin-dike model) and its horizontal derivative (contact model). The tests of clustering and other relevant parameters are conducted. In our experience, every new study area requires an extensive testing of all calculation parameters to 'tune up' to the specific structural-magnetic environment and quality of the magnetic data. For final visualization of resulting solutions on depth cross-sections we usually select one of several available versions that shows all basement indicators most clearly.

Another important feature of our approach is that the magnetic profiles are also extracted from the gridded data with the orientation of profiles selected to be orthogonal to the strike of the dominant magnetic anomalies in the survey area. The resulting decrease in lateral resolution due to reduced sampling proved to be negligible for the purposes of the basement depth calculations. The additional benefits of such grid-extracted

profiles are 1) this complementary dataset eliminates a need for the strike correction and adjustment of calculated depths in case of oblique line direction and 2) low-pass filtering by the gridding process itself suppresses very high frequencies in the original line data. These high frequencies are a combination of noise, residual cultural effects and magnetic signal related to topography.

We use the reduced-to-pole magnetic grids to extract the profiles from the gridded magnetic data. The general theory of the Werner method does not require a reduction to the Magnetic Pole (RTP) to calculate magnetic source depth solutions. However, we have found that quite often the use of the RTP magnetic field profiles produces less noisy and more consistent alignments of depth solutions where the basement indicators are better visible.

We also use culturally edited data (Hassan *et al*. 1998) when there are significant magnetic anomalies due to man-made structures. Cultural anomalies are often sharp spikes. Because spikes are broadband in their frequency content, such anomalies can introduce small residual long-wavelength components into the magnetic field being analysed.

The critically important part of our approach is a selection of clustering parameters. The increased number of calculating windows can result in overpopulation of cross-sections with 'noise' depth solutions that obscure identification of basement indicators. Clustering is a standard procedure often imbedded into calculation algorithms to suppress 'noise' solutions generated by these algorithms. The concept of clustering is that all calculated depth solutions within a pre-selected radius are summarized by their median values of X (location) and Z (depth) once a requirement of their minimum number is met. For example, a tight cluster 1000 m/100, applied to the 2D model calculated depth solutions (Fig. 1), has median values of solutions that fall into the circle with a radius of 1000 m on the condition that a minimum number of solutions within the cluster volume is 100 or more. Clusters with fewer solutions are rejected.

We also use a wide range of other techniques for calculating depths to magnetic sources as independent checks on our interpretation. They include 3D Euler deconvolution (Reid *et al.* 1990) and manual or graphic methods (straight-slope, Peters half-slope, Bean-ratio and others) used for our depth estimates at locations where the magnetic anomalies seem to be undisturbed by interference and intra-sedimentary magmatic intrusions/volcanics. These are good techniques to check the depth range of solutions obtained from the automated 2D Werner calculations and make a more substantiated choice in case of ambiguity in the basement depth level.

The working concept of our approach is based on a) three corroborating types of evidence, generally defined as the 'geologic', 'magnetic' and 'synthetic modelling' evidences, b) use of both empirical basement indicators and independent estimates of basement depth (well control and acoustic basement depth from seismic data) and c) integration with the Bouguer gravity.

Lateral heterogeneity of magnetization is a necessary precondition for the presence of magnetic anomalies. The magnetic anomaly of exploration interest can be defined as a response of the magnetic field to a lateral change in magnetic susceptibility. If there is no change, then there is no anomaly. And every magnetic anomaly, for the purposes of automated calculations of its source's depth, can be approximated with simplified source geometry (thin-dike, thin-sheet, contact, etc.) that is used in a calculation algorithm.

Accordingly, the 'geologic' evidence comes from recognition of differences between the metamorphic/magnetic basement and sedimentary cover in their origins, tectonic histories, lithologies and magnetic properties. These differences result in different patterns of lateral magnetic heterogeneity associated with faults, fracture zones, porosity, igneous intrusions, erosional truncations, subcrop edges and other structural discontinuities. Among other contributors to these differences are the hydrothermal fluids, also called 'juvenile water' (Neuendorf *et al.* 2005, p. 346), produced in large quantities by the process of magma cooling from its liquid state into the solid one. We hypothesize that the abnormally high pressure and temperature of magmas push these fluids into the sedimentary section to open and fill-in faulted, fractured and porous sedimentary rocks and enter into chemical reactions to precipitate magnetic minerals by a hydrofracturing process similar to that described by Williams *et al.* (1999).

An alternative to intra-sedimentary magnetic heterogeneity due to chemical processes is the juxtaposition of sedimentary layers differing in their thickness, depth of occurrence and magnetic susceptibility (Grauch, Hudson and Minor 2001; Grauch *et al.* 2006; Grauch and Hudson 2007). Such situations occur where volcanogenic sediments are present (e.g., rift environments) but they also occur where some layers have significant iron content (e.g., the area around the Peace River Arch in Alberta, Canada, has iron rich sediments in the Mesozoic and lower Tertiary section). In our experience, this model applies to a wider range of environments that has been generally recognized. All together, the differences in lateral magnetic heterogeneity make a basis for the presence of different magnetic source geometries in the basement and sedimentary cover.

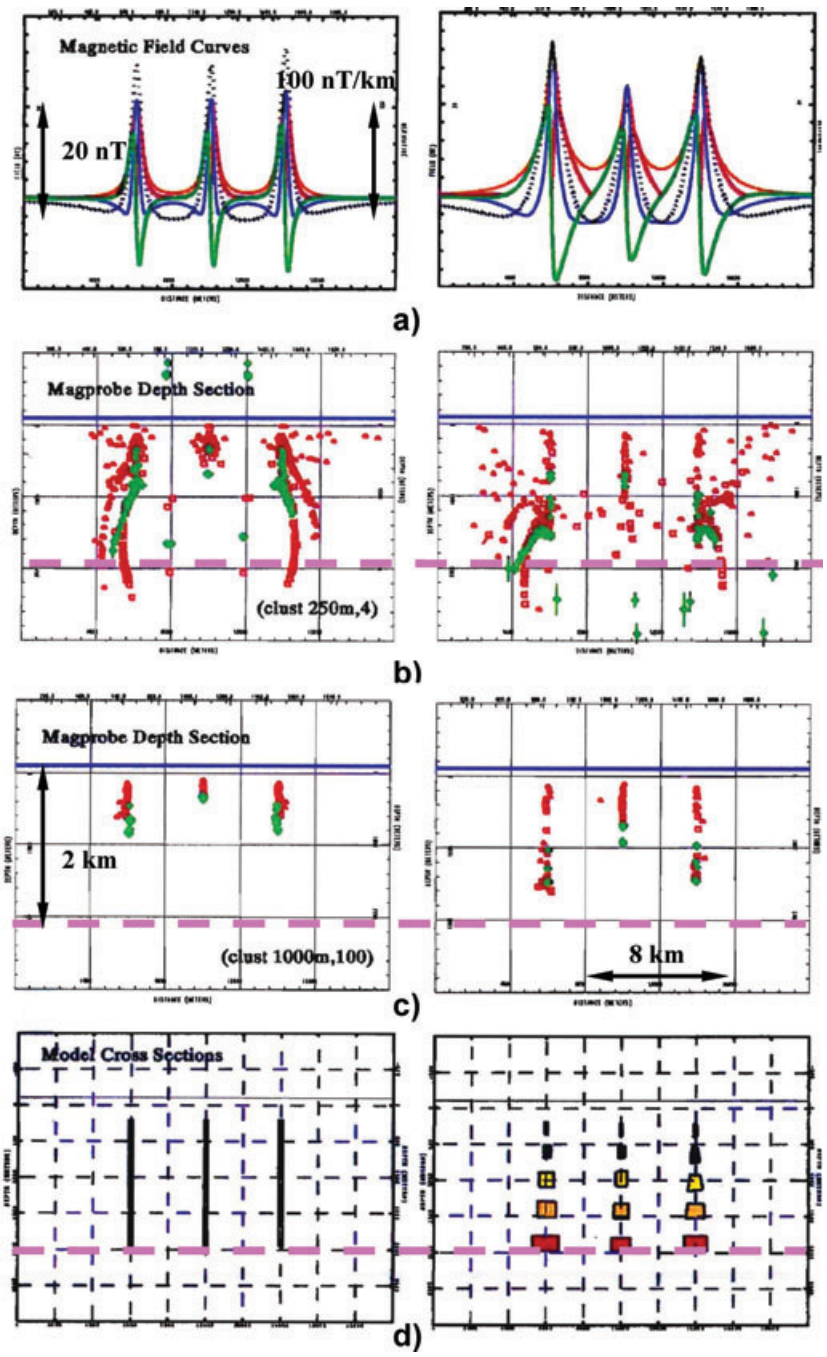

Figure 1 Model simulation of clustered magnetic source depth solutions with three intra-sedimentary dikes (modified from Peirce *et al*. 1999). a) Magnetic fields and their derivatives for three homogeneous dikes on the left and three heterogeneous dikes on the right. The calculated magnetic field is dotted black, its horizontal derivative/gradient – solid green/red, vertical derivative – solid blue, total gradient – orange, b) cross-sections with the Werner deconvolution (red) and Euler deconvolution (green) depth solutions, obtained using less tight (250 m / 4) clustering parameters, for the homogeneous (left) and heterogeneous (right) dikes, c) cross-sections with the Werner deconvolution (red) and Euler deconvolution (green) depth solutions, obtained using more tight (1000 m/100) clustering parameters, for the homogeneous (left) and heterogeneous (right) dikes and d) model cross-sections with homogeneous dikes (left) and heterogeneous dikes (right). Vertical and horizontal scales are the same for all depth cross-sections (black double-head arrows, Fig. 1c). Dashed pink line shows the level of dike bottoms below sensor elevation (dark blue line). Vertical scales of the magnetic fields and their derivatives are shown in nanoTeslas (nT) and nT/km and referenced with black double-head arrows (left panel, Fig. 1a).

The 'geologic' evidence confirms the presence of differences in the lateral magnetic heterogeneity and, hence, magnetic source geometries between the magnetic basement and sedimentary cover. Once different source geometries have been confirmed, then a conclusion can be made that their approximation with the same simplified geometry (thin-dike/thin-sheet or magnetic contact in 2D Werner deconvolution algorithm) will produce different distributions of the calculated magnetic source depth solutions above and below the magnetic basement surface.

The 'magnetic' evidence comes from relatively recent discoveries of new types of magnetic anomalies generated by sources within the sedimentary section. The release of the global positioning system (GPS) into commercial application

made it possible to acquire airborne magnetic data along closely spaced flight lines that allowed making grids with short-wavelength anomalies that were undetectable with wide line spacing. From a long list of publications related to the intra-sedimentary sources and anomalies, we refer the readers to several papers: intra-sedimentary igneous intrusions (Brown, Platt and McGrandle 1994; Kjarsgaard and Davis 1994); secondary magnetization along fault zones (Gunn 1997; Peirce *et al.* 1998); juxtaposition of layers with differing magnetization (Grauch *et al.* 2001 and 2006; Grauch and Hudson 2007); continuous magnetic horizons (Abaco and Lawton 2003); magnetic formations offset by faults (Grauch *et al.* 2001; Goussev *et al.* 2003) and intra-sedimentary magnetic source depth solutions associated with subsurface erosional truncations and faults (Peirce *et al.* 1998; Goussev *et al.* 1998; Glenn *et al.* 2002).

The 'magnetic' evidence confirms the existence of a) wide variety of intra-sedimentary sources, b) detectable intra-sedimentary anomalies and c) intra-sedimentary magnetic source depth solutions. The separation of intra-sedimentary depth solutions from or connection with the intra-basement depth solutions depends on lateral resolution of the basement and sedimentary source geometries and their continuity across the basement surface or truncation at it.

The 'synthetic modelling' evidence is illustrated by three examples: 1) 2D magnetic modelling and calculation of the Werner deconvolution magnetic source depth solutions with three intra-sedimentary homogeneous and heterogeneous dikes (Peirce *et al.* 1999), 2) 2D magnetic modelling and calculation of the Werner deconvolution magnetic source depth solutions with two intra-sedimentary and three intra-basement heterogeneous dikes and 3) application of the methodology described in this paper for 3D Bishop Model by Hassan (2006) and Hassan, Charters and Peirce (2007).

Jain (1976) was the first to show that multiple runs of automated calculations of 2D Werner depth solutions with variable length moving windows over an uniformly magnetized vertical dike produced a vertical dispersion of depth solutions that formed an artificial 'tail' aligned downward from the dike's top. In a 'Round Table' discussion (Peirce *et al.* 1999), the 'tails' associated with three uniformly magnetized (homogeneous) dikes were reproduced and, in addition, three non-uniformly magnetized (heterogeneous) dikes with their susceptibilities and widths increasing with depth were modelled to simulate a geologically plausible approximation of a magnetized fault or fracture zone (Fig. 1). The magnetic susceptibility of the homogeneous dikes was 500 microcgs and for the heterogeneous dikes it varied from 200 m to 1000 microcgs. The calculated magnetic fields and their derivatives are shown on the upper panel (Fig. 1a). The width of the homogeneous dikes was 200 m and for heterogeneous dikes it varied from 200 m to 2000 m (Fig. 1d). With less tight clustering parameters of 250 m as the radius of clustering and 4 as the minimum number of depth solutions to cluster, the depth solutions are noisy and dispersed along the entire depth extent of both homogeneous and heterogeneous dikes and beyond (Fig. 1b). With tighter clustering parameters of 1000 m as the radius of clustering and 100 as the minimum number of depth solutions to cluster, the difference in appearance of depth solutions is very significant: noise is completely suppressed for both the homogeneous and heterogeneous dikes, vertical dispersion is reduced to about half the extent of the centre heterogeneous dike and about $^3/_4$ of the extent of two other heterogeneous dikes (Fig. 1c).

Figure 2 shows the results of the application of our method for a 2D synthetic model with two heterogeneous intra-sedimentary dikes / magnetized faults and three heterogeneous intra-basement dikes (lower panel). The model length is 36 km. Lateral separation of dikes is about 6 km. Basement depth is 2000 m. The widths of intra-sedimentary dikes vary from 0 m to 200 m (dike on the right) and 360 m (dike on the left). The widths of intra-basement dikes vary from about 100 m to 250 m. Magnetic susceptibility of the sedimentary section is 50 microcgs; susceptibility of basement is 1500 microcgs; susceptibilities of intra-sedimentary dikes vary from 100 m to 900 microcgs (dike on the left) and 1500 microcgs (dike on the right). The susceptibilities of intra-basement dikes vary from 2200 microcgs to 3200–3800 microcgs. The magnetic field calculated for this model (inclination 90°, declination 0°) is shown on the upper panel with its maximum values at about 2.4–2.6 nT.

The middle panel of Fig. 2 shows the results of the application of 2D Werner deconvolution with variable length moving windows over this synthetic model. Before running the multiple cycles of calculations, the magnetic field was re-sampled from original 600 m to 20 m (upper panel). The vertical scale is in nanoTeslas (nT) on the left and nT/km on the right for derivatives. The horizontal scale is in metres (upper row) and acquisition reference units (fiducials, lower row). The calculating window length varied from 500 m to 36 km with a variable increment. Clustering parameters were 1000 m/100 (i.e., 1000 m as the radius of clustering and 100 depth solutions as the minimum threshold of clustering). The depth solutions are shown as black vertical crosses. Their size depends on the length of the calculating window that was used to obtain depth solutions: the larger the window, the bigger

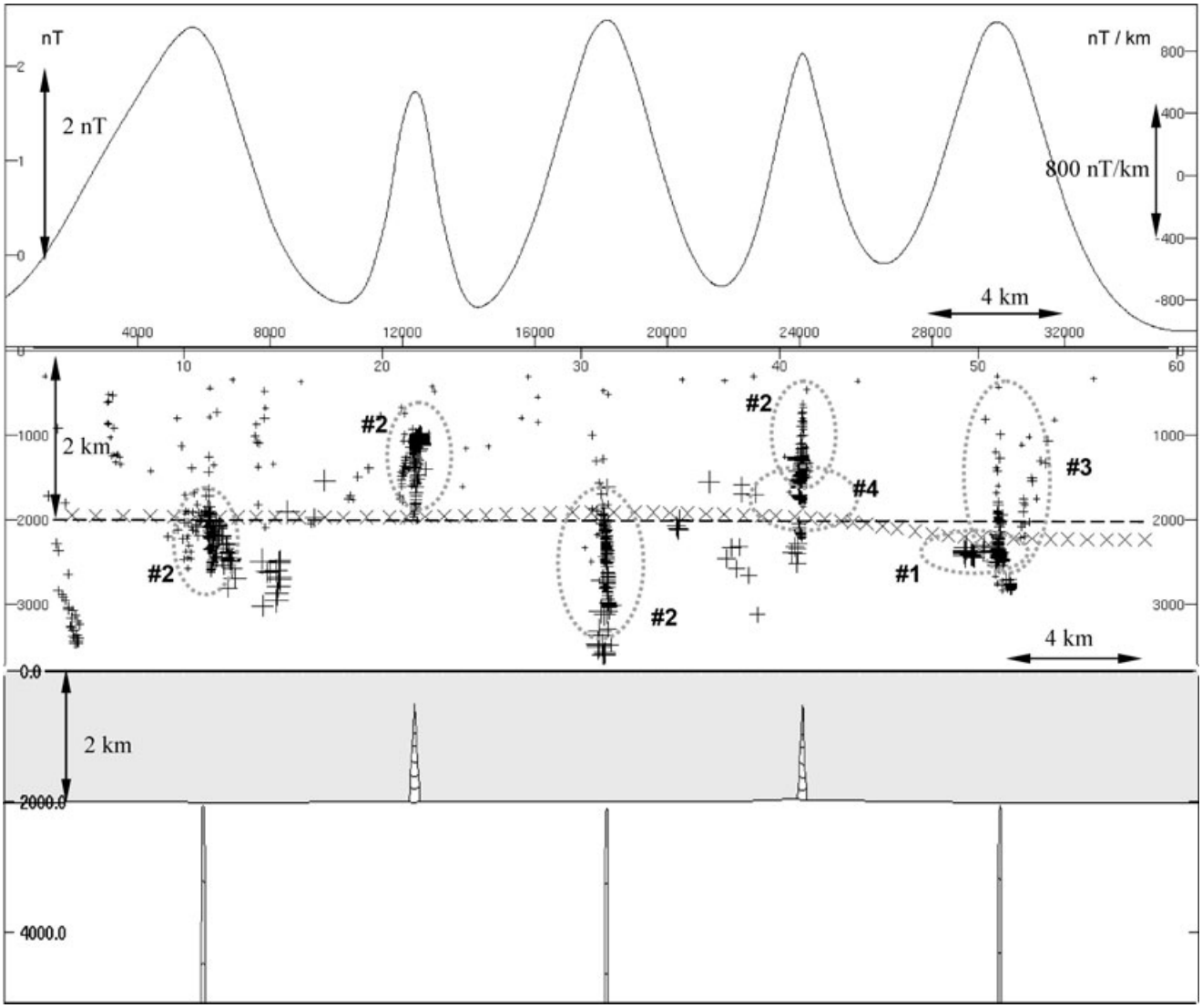

Figure 2 2D magnetic modelling and calculation of the Werner deconvolution depth solutions with two intra-sedimentary and three intra-basement heterogeneous dikes. Upper panel: model calculated magnetic field with lateral increment of 20 m. Vertical scale is shown in nanoTeslas (nT) on the left and in nT/km for derivatives on the right. Middle panel: depth cross-section with the Werner deconvolution depth solutions (black vertical crosses), basement indicators (in grey dotted ellipses), basement correlation (grey diagonal crosses) and basement depth (black dashed line at 2000 m). Indicators are labelled in accordance with types shown in Fig. 4. Vertical and horizontal scales are in metres. Horizontal scale is also shown in the acquisition reference units (fiducials, lower row). Lower panel: 2D magnetic model with two intra-sedimentary and three intra-basement heterogeneous dikes: basement is white, sedimentary section is grey; basement depth is 2000 m; vertical scale is in metres. Horizontal scale is the same for all three panels. Both vertical and horizontal scales on all panels are also referenced with double-head arrows.

the cross. There is no manual clustering or other editing of solutions; they are shown exactly as they appear on the depth cross-section after completion of all cycles of automated calculations.

Grey dotted ellipses highlight patterns of distributed depth solutions (i.e., basement indicators) that can be identified here. Their numbers are shown in accordance with schematic examples numbered in Fig. 4. The model basement is shown as a dashed line at the depth of 2000 m. Diagonal crosses show the basement horizon correlation as it was done manually along this line using the identified basement indicators. The interpreted basement depth varies from about 1800 m to 2200 m yielding an error estimate at 10% of the actual basement depth (2000 m). Four of six types of basement indicators can be identified on this cross-section: #1, #2, #3 and #4 (Fig. 4).

This synthetic model test sheds some light to the origin of the basement indicators. It appears that when the length of a calculating window begins to include samples from both adjacent anomalies, the input segment of the magnetic field deviates from a reference shape (set of equations), used by the calculating algorithm, and multiple runs of calculations start to generate 'noise' solutions in addition to the 'regular' alignments of solutions associated with heterogeneous dikes. This 'noise' has repeatable components that group into specific patterns of depth solutions like near-vertical or lateral alignments, clouds, gaps, etc. Probably, a similar effect takes place with the real case magnetic data when a simplified approximation of sources, used for automated calculation of magnetic source depth solutions, does not match their actual subsurface geometry.

The length of the clustered intra-sedimentary alignments is a function of several variables that include an increase in the dike's width with depth, the degree of the dike's heterogeneity (susceptibility contrast), the lateral separation of dikes (close spacing results in reduced alignments, see Fig. 1) and the clustering parameters. Accordingly, the Werner depth solutions can truncate above, below or at the dike's bottom (Figs 1 and 2). In our experience, the clustered solutions usually truncate above the dike's bottom making an upper constraint for basement horizon correlation.

Figure 3, modified from Hassan (2006), shows the results of the application of 2D Werner deconvolution with variable length moving windows for the magnetic contact approximation of magnetic sources in 3D Bishop Model (Reid, Fitzgerald and Flanagan 2005) and interpretation of its magnetic basement depth using basement indicators described in this paper (Fig. 4).

The Bishop Model basement depth structure is shown in Fig. 3(a). The calculated magnetic field of this model is shown in Fig. 3(b). The grid of difference between the Bishop Model magnetic basement depth and the basement depth interpreted using 3D visualization of calculated depth solutions (Rhodes and Peirce 1999) is shown in Fig. 3(c). The difference between basement depth in the Bishop Model and the one obtained from line-by-line correlation of the basement horizon using basement indicators varies from about –1500 m to about +900 m with dominant values at the range of about ±800–900 m. Figure 3(d) shows the example of a depth section along the north-south oriented interpretation line in the middle of the Bishop Model (Fig. 3b) that incorporates 2D Werner deconvolution magnetic source depth solutions calculated using our multiple window approach with the magnetic contact approximation of source geometry. The green solid line is the Bishop Model magnetic basement and the yellow solid line is the interpreted magnetic basement. The depth section shows a distinct and repeated pattern of truncations of vertical alignments of calculated intra-basement depth solutions at the top of magnetic basement. This pattern is used as one of the basement indicators in our method (#2 in Fig. 4).

The main conclusions from the results of synthetic modelling are 1) 2D modelling proves that empirically derived basement indicators can be reproduced in the synthetic model composed of the 'thin-dike' source geometries (Figs 1 and 2) and 2) the 3D Bishop Model test proves that basement indicators can be reproduced in the synthetic model that has only a few 'magnetic contact' source geometries and no intra-basement faults. These indicators have the repeatability necessary for successful interpretation of the magnetic basement over large areas (Fig. 3).

On the technical side, 2D modelling tests demonstrate that a) both uniformly and non-uniformly magnetized dikes produce vertical alignments or 'tails' of clustered depth solutions when multiple variable length moving windows are used for calculations, b) alignments of depth solutions are sensitive to the magnetic properties, source geometry and selection of clustering and other calculation parameters and c) vertical heterogeneity in dike magnetization can produce a longer vertical alignment of depth solutions as compared to the uniformly magnetized dike.

2D Werner deconvolution cannot resolve vertically heterogeneous parts of dikes but the heterogeneity itself seems to be instrumental in producing additional depth solutions that enhance their vertical alignments associated with all three heterogeneous dikes. Multiple sliding windows of different length seem to work similar to different filters applied to the data.

We consider the truncated-bed model (Grauch *et al*. 2001) as an alternative and possibly more plausible geologically intra-sedimentary model then the thin-dike model. We acknowledge that it is difficult to imagine getting enough volume of high magnetic susceptibility into an intra-sedimentary 'dike' in order to create a measurable magnetic anomaly at the surface unless the 'dike' is in fact igneous in origin. However, our empirical observation is that the distribution of 2D Werner deconvolution depth solutions often resembles the thin-dike model with a vertically heterogeneous set of sources.

Empirical basement indicators were developed from the experience of a visual analysis of distributions and alignments of the Werner deconvolution magnetic source depth solutions near the wells that penetrated the crystalline/metamorphic basement. The analysis revealed specific patterns of changes in distributions and alignments of calculated depth solutions

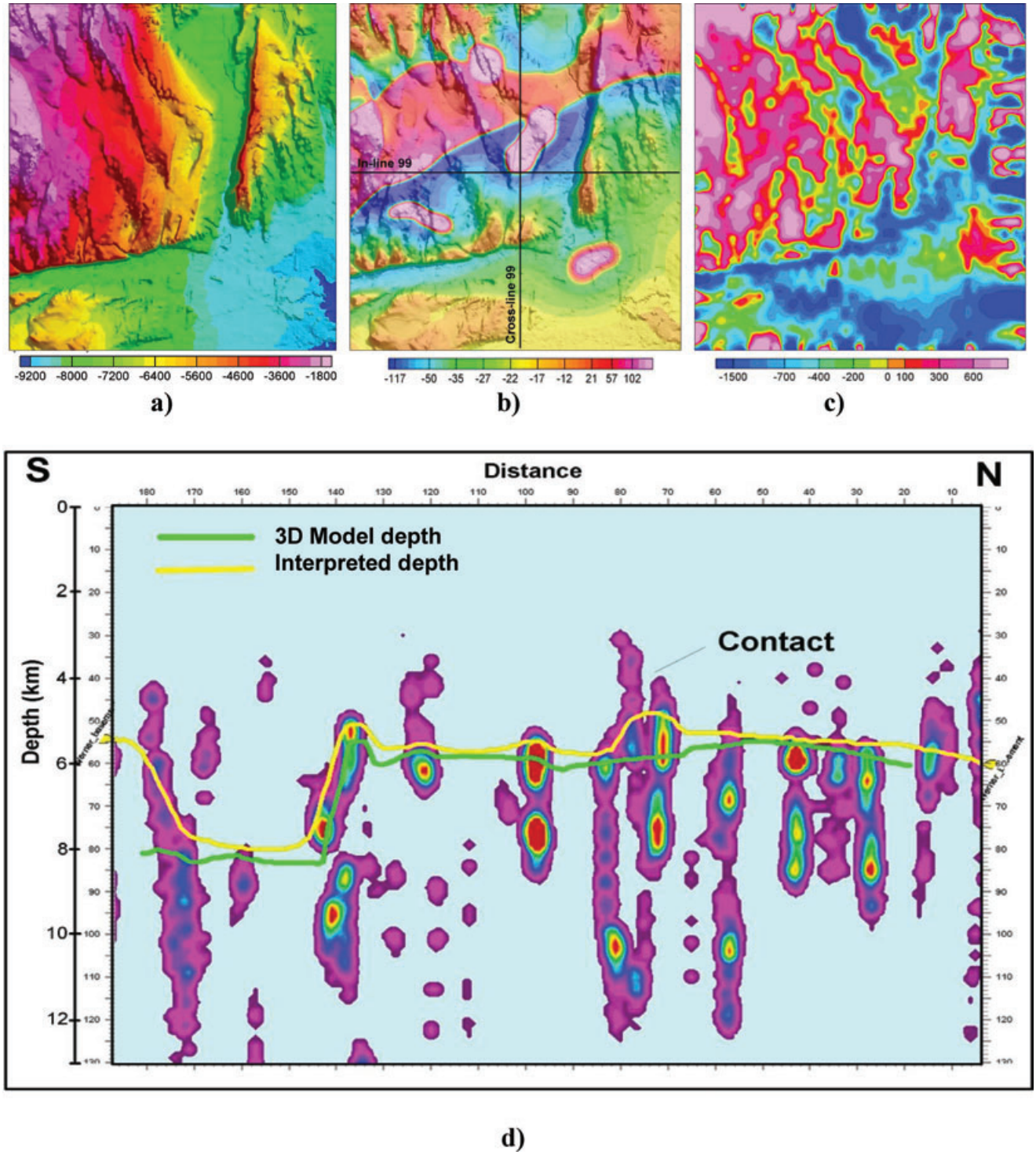

Figure 3 Application for 3D Bishop Model (modified from Hassan 2006). a) Bishop model magnetic basement depth, b) magnetic field calculated from the Bishop model, c) difference between magnetic basement depth of the Bishop model and magnetic basement depth interpreted with the use of basement indicators and d) north-south depth cross-section with calculated magnetic source depth solutions and basement correlation (Bishop model basement is green and interpreted basement is yellow).

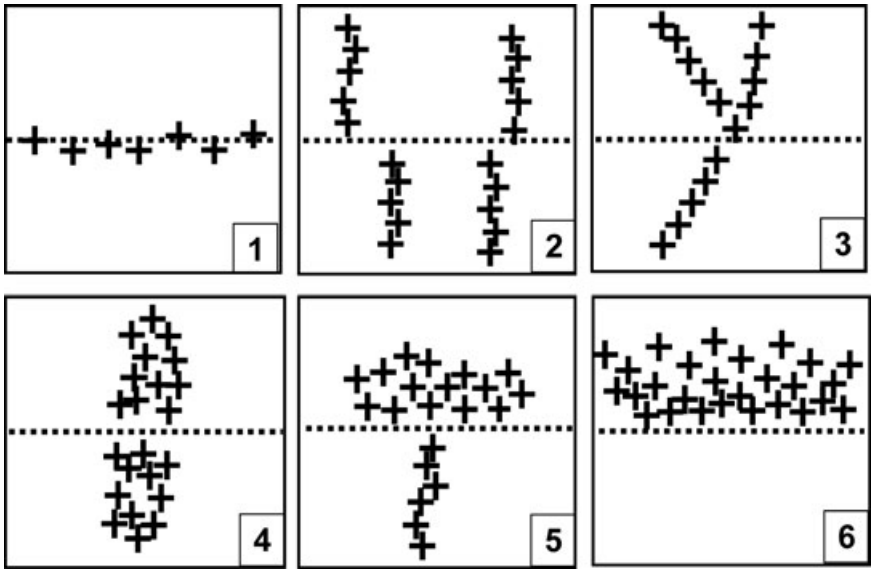

Figure 4 Empirical basement indicators: 1 – 'lateral alignment', 2 – 'truncation', 3 – 'change of dip', 4 – 'gap', 5 – 'alignment into cloud', 6 – 'bounded noise'. Magnetic basement is shown as a black dotted line.

across the surface of magnetic basement. The consistency and repeatability of such changes made it possible to develop the following empirical set of basement indicators for identification and correlation of the magnetic basement (Fig. 4):

1 'lateral alignment' – depth solutions align laterally along the basement surface;

2 'truncation'– vertical or near-vertical alignments of intra-sedimentary and intra-basement depth solutions truncate along the basement surface;

3 'change of dip'– alignments of depth solutions abruptly change their apparent dip, sometimes, to the opposite direction across the basement surface;

4 'gap' – zone without depth solutions between clusters of intra-sedimentary and intra-basement solutions;

5 'alignment into cloud'– intra-basement vertical alignment of depth solutions transforms into a cloud of solutions across the basement surface;

6 'bounded noise' – laterally extended cloud of noise solutions is bounded from below by the basement surface.

It should be noted here that simplified images of basement indicators in Fig. 4 imply their mirror character, i.e., criteria #2, #3, #5 and #6 can be observed above and below the basement surface.

The integration of the Bouguer gravity into the process of basement interpretation comes from a proven fact that every large basement structure, structural high or structural low, has its corresponding Bouguer gravity anomaly, except in cases where the density contrast is close to zero. Obviously, the opposite is not necessarily true: not every Bouguer gravity anomaly is associated with the basement structure. Intra-sedimentary salt and mobile shale structures (diapirs, domes, pillows), thin-skin thrusting, intra-sedimentary high-density basalt lava flows, intra-basement low-density granite intrusions and other elements of the subsurface structure generate gravity anomalies that have no relation to the shape of the basement surface. Accordingly, our integrated approach does not just mimic the Bouguer gravity anomalies in the magnetic basement depth interpretation. With appropriate geological judgment, we evaluate and incorporate them into the process of basement correlation as a source of independent structural information that can be used as a guide for making a choice between two alternative correlations: up or down along the interpreted line. In addition to profiles of the Bouguer gravity anomalies placed on top of interpreted depth cross-sections, the enhancements of the Bouguer gravity field with low- and high-pass filtering and calculation of its residuals and derivatives often help to get a better judgment of the origin of the Bouguer anomalies and their association with interpreted basement structures. As in any interpretation process, there are alternatives in the basement correlation and the Bouguer gravity can help to make a more substantiated choice.

INTERPRETATION EXAMPLES

Six real case examples shown in Figs 5, 6, 8 and 9 were taken from marine acquisition data and the example in Fig. 7 – from high-resolution aeromagnetic data. The magnetic source depth solutions have been obtained with 2D Werner

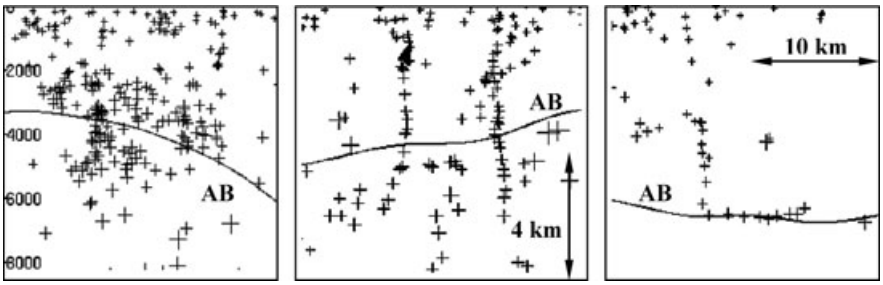

Figure 5 Examples of basement indicators in real data: 'gap' and 'bounded noise' (left), 'change of dip' (centre), 'truncation' and 'lateral alignment' (right). Acoustic basement horizon (AB) is shown as independent overlay. Vertical and horizontal scales are the same for all three examples and referenced with double-head arrows (centre and right examples).

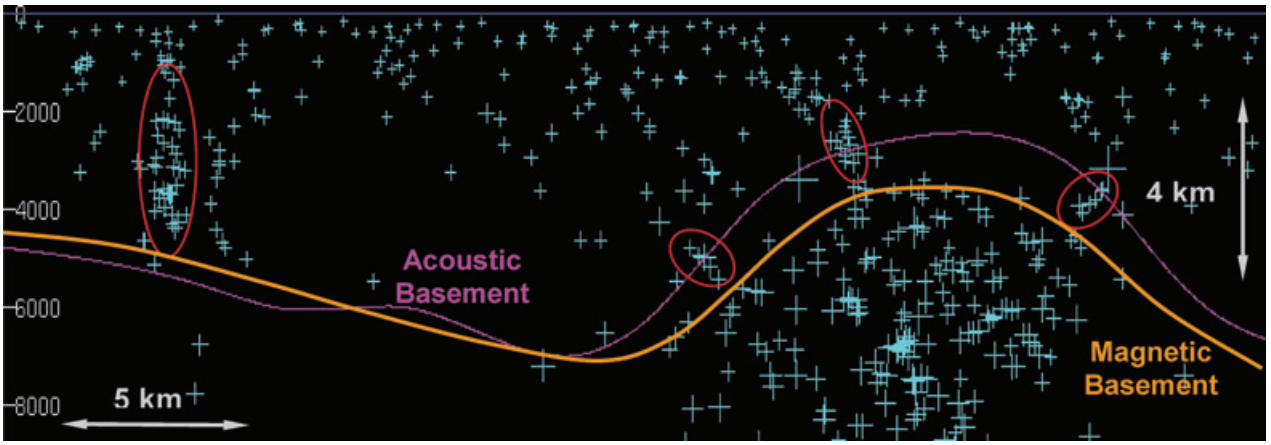

Figure 6 Basement horizon correlation using basement indicators (in red ellipses): 'truncation' on the left and three 'truncations' and 'bounded noise' on the right. Acoustic basement horizon is shown in magenta and correlated magnetic basement horizon in orange.

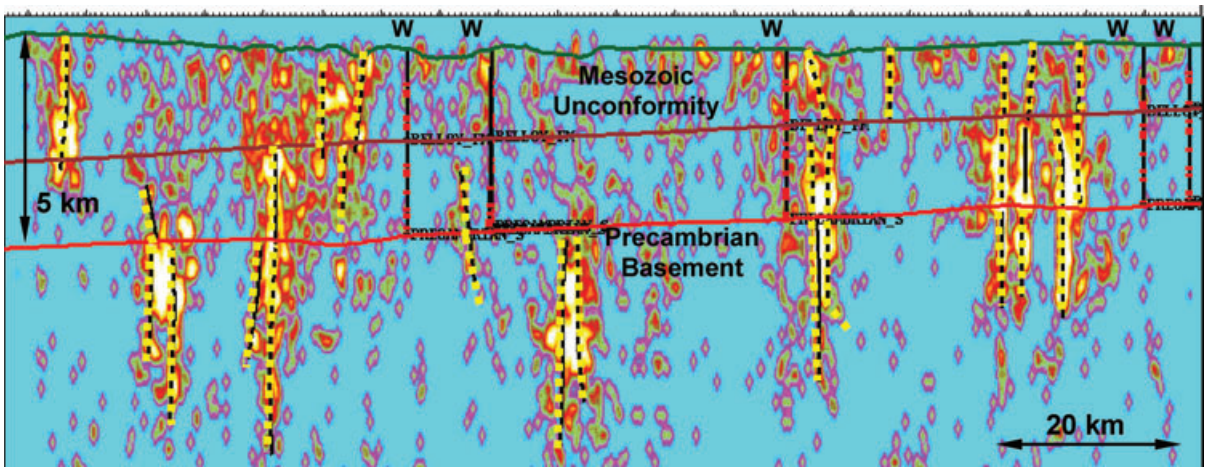

Figure 7 Basement indicators and Precambrian basement horizon (red) on the depth cross-section overlain with Mesozoic Unconformity horizon (brown) and five Precambrian wells ('W'). Yellow dotted lines show interpreted alignments of depth solutions. Horizontal and vertical scales are referenced with double-head arrows.

deconvolution in its option for the total field and thin-dike approximation of magnetic sources for all examples except for Fig. 7 where both 'thin-dike' and 'magnetic contact' approximations were used. There is no manual clustering of calculated depth solutions in our applications. The clustered depth solutions are shown as '+' signs. Their size depends on the length of the calculation window: the larger the window, the bigger their size.

Figure 5 shows three examples of the 2D Werner deconvolution depth cross-sections overlain with the seismic acoustic basement horizon (AB). The purpose of these examples is to show the specific patterns in distribution and alignments of depth solutions across a real geological boundary – acoustic basement. All three cross-sections have the same vertical scale in metres below sea level shown on the left image. There are five basement indicators here (see also Fig. 4): 'gap' and 'bounded noise' (left image), 'change of dip' (middle image), 'truncation' and 'lateral alignment' (right image). Subtle but consistent in appearance, the indicators are recognizable against the background of noise depth solutions attenuated by tight clustering. In these examples, the acoustic basement, as an independent overlay, is coincident with the interpreted magnetic basement.

Figure 6 shows an example of the magnetic basement interpretation constrained by the acoustic basement horizon. There are five basement indicators (four shown in red ellipses): one 'truncation' (indicator #2) in the left part of the cross-section and three 'truncations' and the fifth indicator ('bounded noise', #6) in the right part, where the basement uplift is formed by a prominent igneous intrusive body. The presence of an igneous intrusion here was confirmed by analysis of the reduced-to-pole magnetic field and its derivatives. Note the distinctly different distributions of calculated depth solutions within the igneous body and outside its upper boundary. The acoustic basement (magenta) is about 1.5 km shallower than the interpreted magnetic basement (orange) on the right and practically coincident with it in the left part of the cross-section. The magnetic basement depth in the gap between indicators on the left and on the right is defined by its correlation on two acquisition lines that are orthogonal to the line fragment shown on this figure.

Figure 7 shows basement indicators at the depth cross-section from the Peace River Arch that was extracted from a 3D visualization volume (Rhodes and Peirce 1999). The section is overlain with two interpreted horizons, Precambrian basement and the Mesozoic unconformity, and five wells that penetrate the Precambrian basement. The presence of five basement wells along with the basement indicators (mostly, #2 types) between them and beyond makes the basement interpretation on this cross-section quite obvious. The purpose of this example is to show the distributions and alignments of calculated 2D Werner deconvolution depth solutions in the vicinity of basement penetrating wells (W). Another purpose is to illustrate a limitation of our approach when similar indicators appear at a much shallower level of the Mesozoic unconformity. In frontier areas, where basement wells are few or missing and seismic acoustic basement is not available, the lack of independent constraints increases the ambiguity in identification of the basement indicators and their correlation. In such cases, the conventional magnetic source depth calculations techniques like 3D Euler deconvolution and manual/graphic methods can provide additional information to minimize the depth range ambiguity.

Figures 8 and 9 show the examples of basement horizon correlation on the depth cross-sections integrated with the Bouguer gravity profiles and acoustic basement horizon (Fig. 8) and without it (Fig. 9). In the situation of ambiguity of lateral correlation (i.e., shallower or deeper along the interpreted cross-section), both 'alternative correlation' options (solid orange line in Fig. 8 and dashed line in Fig. 9) are not in agreement with a trend of lateral changes in the corresponding Bouguer gravity profiles and we use this observation to make a choice between two alternative basement correlations.

In Fig. 8, the basement indicators (in red ellipses) were identified both along the acoustic basement horizon (magenta) and below it. There is ambiguity in the selection of basement indicators with a choice between a structural high (along the acoustic basement) and structural slope (marked as 'alternative correlation' and solid orange line). The Bouguer gravity profile guides the correlation of magnetic basement in the most probable direction of a structural high. Accordingly, our interpretation of the magnetic basement on this cross-section is shown in solid white colour. Such ambiguity in correlating the magnetic basement is not surprising as the correlation of the acoustic basement on seismic data can be a highly interpretive exercise too. Furthermore, the conversion of seismic data to depth can be inaccurate and potentially misleading unless there is good velocity control. These uncertainties increase even more in structured areas where ray tracing is required to achieve a reasonable time-to-depth conversion of the seismic data.

In Fig. 9, with quite distinct basement indicators and without acoustic basement available to constrain the correlation, two interpretations of the magnetic basement depth are equally probable in the middle of the cross-section: structural high (marked as 'alternative correlation' and dashed line) and structural low (solid line with diagonal crosses). The Bouguer gravity profile and, in particular, its long-wavelength component eliminate this ambiguity in favour of a structural low.

The basement indicators, similar to the interpreted ones, can be identified in Fig. 9 at the shallower depth range of about 3–4 km. The same situation was shown in Fig. 7 and explained as a limitation of our approach. However, with water depth

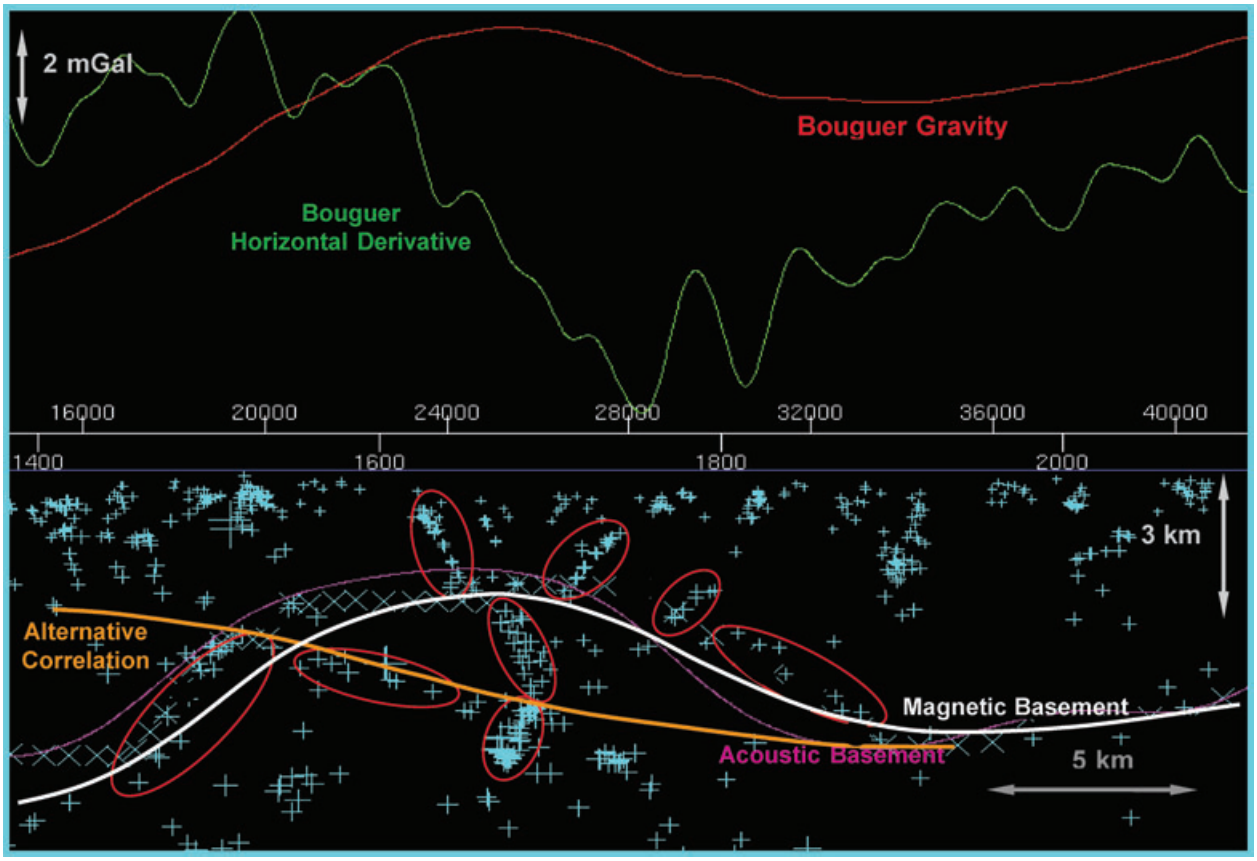

Figure 8 Examples of basement indicators (in red ellipses) and basement horizon correlation on the depth cross-section with acoustic basement horizon (magenta). Alternative correlation is shown in orange. Bouguer gravity profile (red) and its horizontal derivative (green) are shown on the upper panel. Magnetic basement interpretation is shown in white. Horizontal scale is shown in metres (upper row) and acquisition reference units (fiducials, lower row). Vertical scales for the Bouguer gravity and depth are referenced with grey double-head arrows (upper left and lower right).

of about 800–1000 m in this area and its location within the known rifted continental margin, the sedimentary thickness of about 2–3 km is geologically improbable here. Based on this appropriate geological judgment, we can eliminate the 'depth range' ambiguity in identification and correlation of the basement indicators.

CONCLUSIONS

Based on the above considerations, illustrated with three synthetic modelling and seven real case examples, the following conclusions were made:

1 Crystalline/metamorphic basement and sedimentary cover have recognizable differences in magnetic source geometries that can be visualized by distributions and alignments of 2D Werner deconvolution magnetic source depth solutions.

2 The 2D and 3D modelling tests prove that the empirically derived basement indicators can be reproduced in the synthetic models with both 'thin-dike' and 'magnetic contact' source geometry approximations used in 2D Werner deconvolution method.

3 The 3D Bishop Model test proves that empirical basement indicators have the repeatability necessary for successful interpretation of the magnetic basement over large areas.

4 Empirical basement indicators closely correlate with the metamorphic/crystalline basement onshore and seismic acoustic basement in offshore areas.

5 The empirical set of six criteria or basement indicators has been developed for identification and correlation of the magnetic basement.

6 Integration with the Bouguer gravity (profiles and grids) provides additional information for more substantiated choice between alternative basement correlation options in areas where well control and other interpretation constraints are limited or non-existent.

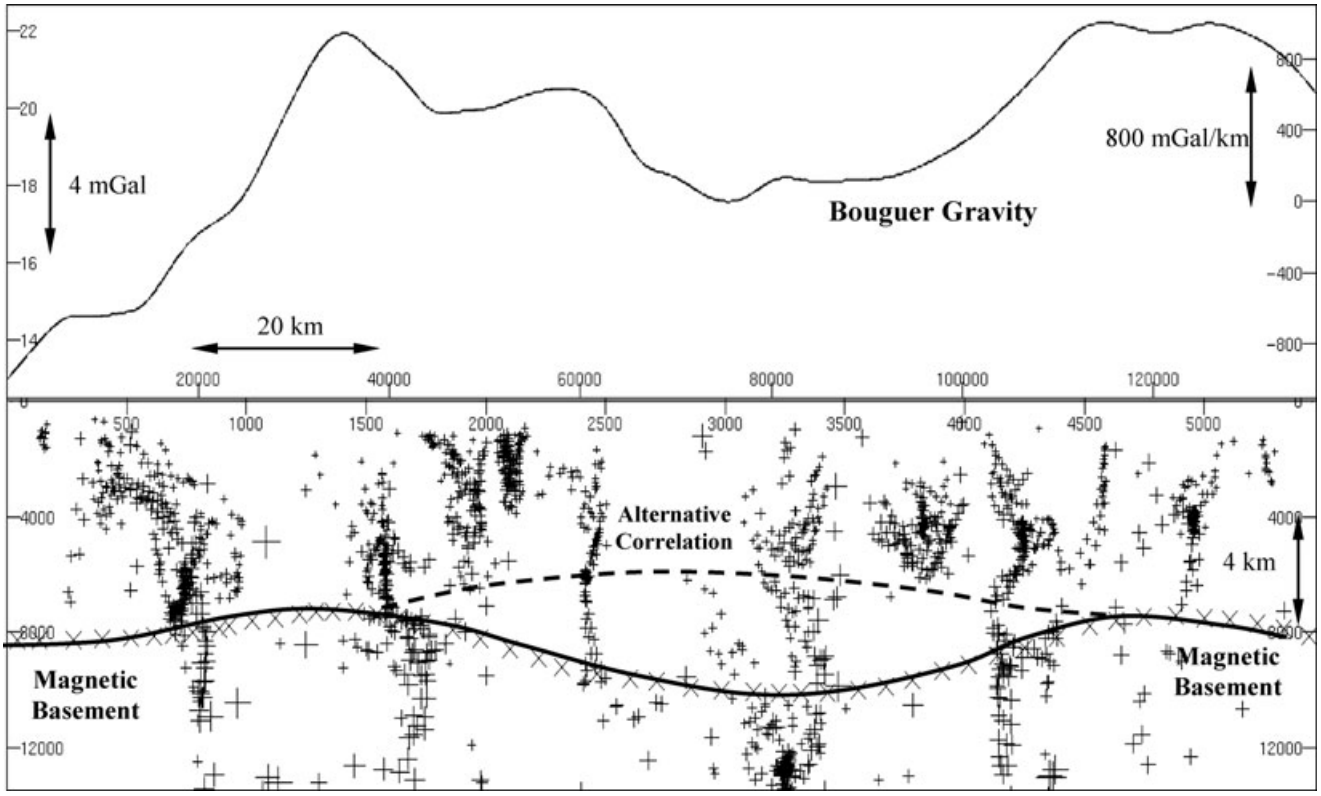

Figure 9 Basement horizon correlation on the depth cross-section with the Bouguer gravity profile (upper panel). Magnetic basement horizon is shown in solid black with diagonal black crosses and alternative correlation is shown as dashed black line. On the upper panel, left vertical scale is in milliGals (mGal) and right vertical scale is in mGal/km for derivatives. On the lower panel, horizontal scale is in metres (upper row) and acquisition reference units (fiducials, lower row). Vertical scale on the depth cross-section is in metres. Both scales are also referenced with double-head arrows.

7 The presented method of magnetic basement interpretation is based on three types of corroborating evidence ('geologic', 'magnetic' and 'synthetic modelling') and the use of empirical basement indicators in integration with the Bouguer gravity.

As compared to the traditional magnetic basement interpretation, our integrated approach has many unique features.

First, it is based on the use of increased number of variable length moving windows and tight clustering to improve the visualization of depth solutions, generated by real magnetic sources, against a background of spurious depth solutions generated by noise in the data and misplaced depth solutions ('tails') generated by the 2D Werner deconvolution algorithm.

Second, in addition to the magnetic profiles along the acquisition lines, the profiles for calculation of depth solutions are extracted from the reduced-to-pole grids with profile directions oriented perpendicular to the dominant magnetic grain in the survey area.

Third, instead of just one basement indicator used in the traditional interpretation (i.e., calculated depths to the sources of observed dominant anomalies), six empirical basement indicators are used to provide a higher accuracy and resolution of elements of the basement depth structure.

Fourth, along with depth solutions associated with the basement top, the distributions and alignments of intra-sedimentary depth solutions are also taken into consideration to make the basement interpretation more resolvable laterally.

Fifth, the Bouguer gravity profiles and grids are incorporated into the process of basement correlation as independent sources of structure-related information to reduce the ambiguity of correlation where well control and other constraints are limited or non-existent.

Sixth, the magnetic basement is mapped from line-by-line correlation of the basement horizon, not as isolated depth picks, with ties of correlation at line intersections and, hence, higher accuracy of the basement depth interpretation. The importance of this last constraint cannot be over-emphasized to ensure an area-wide consistency and spatial resolution of the interpretation.

As any interpretation method, our approach has its limitations and subject to complications associated with quality of original magnetic data and other objective factors. We believe the concept of making visible the changes in source geometries across the 'basement-sedimentary cover' boundary for the magnetic basement interpretation can be applied to the use of other magnetic source depth estimation techniques, including 2D Euler deconvolution.

ACKNOWLEDGEMENTS

We would like to acknowledge Fugro Gravity & Magnetic Services (FGMS) and GEDCO for permission to publish this paper, Hassan Hassan (FGMS) for permission to use figures from his SEG Workshop Poster, Mark Weber, Rao Yalamanchili and Vsevolod Egorov (FGMS), reviewers Alan Reid, Roman Pasteka and two anonymous reviewers for their critical comments and suggestions that helped to improve this paper and two oil companies that preferred to stay anonymous, for permission to use their data. Thanks also to Bob Charters (GEDCO) for finding an original copy of the 1999 TLE figures so that we could put proper scales on these figures.

REFERENCES

Abaco C.I. and Lawton D.C. 2003. Magnetic anomalies in the Alberta foothills, Canada. 73rd SEG meeting, Dallas, Texas, USA, Expanded Abstracts, 612–615.

Brown G., Platt N.H. and McGrandle A. 1994. The geophysical expression of Tertiary dikes in the southern North Sea. *First Break* **12**, 137–146.

Glenn W.E., Rhodes J.A., Goussev S.A., Benedict M.N., Charters R.A. and Peirce J.W. 2002. Aeromagnetic depth solutions indicate numerous magnetic sources within the sedimentary section in the Western Canada Sedimentary Basin. CSEG, Expanded Abstracts, 132–134.

Goussev S.A., Charters R.A., Hassan H.H., Peirce J.W. and Genereux J. 1998. HRAM fault interpretation using MAGPROBE^{TM} depth estimates and non-traditional filtering. *Canadian Journal of Exploration Geophysics* **34**, 30–39.

Goussev S.A., Charters R.A., Peirce J.W. and Glenn W.E. 2003. Jackpine Creek magnetic anomaly: Identification of a buried meteorite impact structure. *The Leading Edge* **22**, 740–741.

Grauch V.J.S. and Hudson M.R. 2007. Guides to understanding the aeromagnetic expression of faults in sedimentary basins: Lessons learned from the central Rio Grande rift, New Mexico. *Geosphere* **3**, 596–623.

Grauch V.J.S., Hudson M.R. and Minor S.A. 2001. Aeromagnetic expression of faults that offset basin fill, Albuquerque basin, New Mexico. *Geophysics* **66**, 707–720.

Grauch V.J.S., Hudson M.R., Minor S.A. and Caine J.S. 2006. Sources of along-strike variation in magnetic anomalies related to intra-sedimentary faults: A case study from the Rio-Grande Rift, USA. *Exploration Geophysics* **37**, 372–378.

Gunn P.J. 1997. Application of aeromagnetic surveys to sedimentary basin studies. *AGSO Journal of Australian Geology and Geophysics* **17**, 133–144.

Hartman R.R., Teskey D.J. and Friedberg J.L. 1971. A system for rapid digital aeromagnetic interpretation. *Geophysics* **36**, 891–918.

Hassan H.H. 2006. 2D Euler and 2D Werner inversion results in MaFIC are used to map magnetic basement for the Bishop 3D realistic model. 76th SEG meeting, New Orleans, Louisiana, USA, Expanded Abstracts.

Hassan H.H., Charters R.A. and Peirce J.W. 2007. Mapping depth to basement using 2D Werner inversion of High-Resolution Aero-Magnetic (HRAM) data. CSPG-CSEG, Expanded Abstracts, 222–225.

Hassan H.H., Peirce J.W., Pearson W.C. and Pearson M.J. 1998. Cultural editing of HRAM data: comparison of techniques. *Canadian Journal of Exploration Geophysics* **34**, 16–23.

Jain S. 1976. An automated method of direct interpretation of magnetic profiles. *Geophysics* **41**, 531–545.

Kjarsgaard B.A. and Davis W.J. 1994. Eocene magmatism, Sweet Grass Hills: Expression and significance. *Lithoprobe Report* **37**, 234–237.

Ku C.C. and Sharp J.A. 1983. Werner deconvolution for automated magnetic interpretation and its refinement using Marquardt inverse modeling. *Geophysics* **48**, 754–774.

Li X. 2003. On the use of different methods for estimating magnetic depth. *The Leading Edge* **22**, 1090–1099.

Nabighian M.N., Grauch V.J.S., Hansen R.O., LaFehr T.R., Li Y., Peirce J.W.*et al*. 2005. The historical development of the magnetic method in exploration. *Geophysics* **70**, 33ND–61ND.

Neuendorf K.K.E., Mehl J.P. and Jackson J.A. (eds) 2005. *Glossary of Geology*, 5th edn. American Geological Institute.

Peirce J.W., Goussev S.A., Charters R.A., Abercrombie H.J. and DePaoli G.R. 1998. Intra-sedimentary magnetization by vertical fluid flow and exotic geochemistry. *The Leading Edge* **17**, 89–92.

Peirce J.W., Goussev S.A., Charters R.A., Abercrombie H.J., DePaoli G.R. and Pawlowski R. 1999. Round Table discussion. *The Leading Edge* **18**, 211–214.

Reid A.B., Allsop J.M., Granser H., Millet A.J. and Somerton I.W. 1990. Magnetic interpretation in three dimensions using Euler deconvolution. *Geophysics* **55**, 80–91.

Reid A., Fitzgerald D. and Flanagan G. 2005. Hybrid Euler magnetic basement depth estimation – Bishop 3D tests. 75th SEG meeting, Houston, Texas, USA, Expanded Abstracts, 671–673.

Rhodes J.A. and Peirce J.W. 1999. MaFIC – Magnetic Interpretation in 3D using a seismic workstation. 69th SEG meeting, Houston, Texas, USA, Expanded Abstracts, 335–338.

Sheriff R.E. 2006. *Encyclopedic Dictionary of Applied Geophysics*, 4th edn. SEG. ISBN 1560801182.

Werner S. 1955. Interpretation of magnetic anomalies as sheet-like bodies. *Sveriges Geologiska Undersökning, Series C, Årsbok* **43**, No. 6.

Williams W.C., Meissl E., Madrid J. and de Machura B.C. 1999. The San Jorge porphyry copper deposit, Mendoza, Argentina: A combination of orthomagmatic and hydrothermal mineralization. *Ore Geology Reviews* **14**, 185–201.